Biomedical Optics EXPRESS

Stability and instability for low refractive-index-contrast particle trapping in a dual-beam optical trap

Alison Huff, Charles N. Melton, Linda S. Hirst, and Jay E. Sharping*

Physics Department, University of California, Merced, Merced, CA 95343, USA

*jsharping@ucmerced.edu

Abstract: A dual-beam optical trap is used to trap and manipulate dielectric particles. When the refractive index of these particles is comparable to that of the surrounding medium, equilibrium trapping locations within the system shift from stable to unstable depending on fiber separation and particle size. This is due to to the relationship between gradient and scattering forces. We experimentally and computationally study the transitions between stable and unstable trapping of poly(methyl methacrylate) beads for a range of parameters relevant to experimental setups involving giant unilamellar vesicles. We present stability maps for various fiber separations and particle sizes, and find that careful attention to particle size and configuration is necessary to obtain reproducible quantitative results for soft matter stretching experiments.

OCIS codes: (060.2310) Fiber optics; (140.7010) Laser trapping.

References and links

1. A. Ashkin, "Acceleration and trapping of particles by radiation pressure," Phys. Rev. Lett. **24**(4), 156–159 (1970).
2. J. Jass, S. Schedin, J. Ohlsson, U. J. Nilsson, B. E. Uhlin, and O. Axner, "Physical properties of *Escherichia coli* P Pili measured by optical tweezers," Biophys. J. **87**(6), 4271–4283 (2004).
3. K. Gibble and S. Chu, "Laser-cooled Cs frequency standard and a measurement of the frequency shift due to ultracold collisions," Phys. Rev. Lett. **70**(12), 1771–1774 (1993).
4. M. E. Solmaz, R. Biswas, S. Sankhagowit, J. R. Thompson, C. A. Mejia, N. Malmstadt, and M. L. Povinelli, "Optical stretching of giant unilamellar vesicles with an integrated dual-beam optical trap," Biomed. Opt. Express **3**(10), 2419–2427 (2012).
5. S. Sankhagowit, S. H. Wu, R. Biswas, C. T. Riche, M. L. Povinelli, and N. Malmstadt, "The dynamics of giant unilamellar vesicle oxidation probed by morphological transitions," Biochim. Biophys. Acta **1838**(10), 2615–2624 (2014).
6. J. Guck, R. Ananthakrishnan, H. Mahmood, T. J. Moon, C. C. Cunningham, and J. Kãs, "The optical stretcher: a novel laser tool to micromanipulate cells," Biophys. J. **81**(2), 767–784 (2001).
7. J. Guck, R. Ananthakrishnan, H. Mahmood, T. J. Moon, C. C. Cunningham, and J. Kãs, "Optical deformability of soft biological dielectrics," Phys. Rev. Lett. **84**(23), 5451–5454 (2000).
8. P. B. Bareil, Y. Sheng, Y. Chen, and A. Chiou, "Calculation of spherical red blood cell deformation in a dual-beam optical stretcher," Opt. Express **15**(24), 16029–16034 (2007).
9. E. A. Evans, " New membrane concept applied to the analysis of fluid shear-and micropipette-deformed red blood cells," Biophys. J. **13**(9), 941–954 (1973).
10. T. M. Piñón, A. R. Castelli, L. S. Hirst, and J. E. Sharping, "Fiber-optic trap-on-a-chip platform for probing low refractive index contrast biomaterials," Appl. Opt. **52**(11), 2340–2345 (2013).
11. E. Sidick, S. D. Collins, and A. Knoesen, "Trapping forces in a multiple-beam fiber-optic trap," Appl. Opt. **36**(25), 6423–6432 (1997).
12. U. Delabre, K. Feld, E. Crespo, G. Whyte, C. Sykes, U. Seifert, and J. Guck, "Deformation of phospholipid vesicles in an optical stretcher," Soft Matter **11**(30), 6075–6088 2015

#244048 Received 30 Jun 2015; revised 30 Aug 2015; accepted 1 Sep 2015; published 4 Sep 2015

13. E. J. G. Peterman, F. Gittes, and C. F. Schmidt, "Laser-induced heating in optical traps," Biophys. J. **84**(2), 1308–1316 (2003).

Optical trapping occurs when radiation pressure forces from one or more lasers trap microscopic dielectric particles. Since first demonstrated in 1970 [1], optically trapped particles have been of interest in a wide variety of fields, from determining forces applied to *E. coli* with optical tweezers [2] to measuring frequency shifts from colliding cesium atoms cooled using a magneto-optical atom trap [3]. Using these forces, we trap dielectric particles using a dual-beam optical trap as demonstrated by Ashkin [1], where the beams are counter-propagating and are aligned coaxially. These traps have been used to probe the elasticity of soft matter particles, such as giant unilamellar vesicles (GUVs) [4, 5] and red blood cells [6–8], by trapping and stretching the particles to reveal the stress/strain response of the particle membrane.

The use of an optical trap to controllably immobilize and deform GUVs provides a unique method to study biological and synthetic membrane mechanics. Minimal biophysical systems such as the GUV allow basic physical parameters such as elasticity moduli to be measured with the option of adding in additional complexity (different lipids, proteins) in a systematic fashion. This approach complements previous recent studies carried out on whole cells by Guck et al. [6–8]. Recently membrane mechanics have been studied via methods involving direct contact with the membrane, such as micropipette aspiration [9]. While these methods can provide reliable data, they only provide measurements for one area of the membrane, and do not characterize it as a whole. With this in mind, a non-invasive method of testing such as an optical trap is necessary to characterize a bulk response of the membrane due to time-dependent forces. A dual beam optical trap has recently been shown, by our research group, to successfully stretch a GUV [10] well beyond previously reported stretching regimes in similar experimental setups [4]. However, it was shown to be fairly difficult to successfully trap the GUVs between the two fibers.

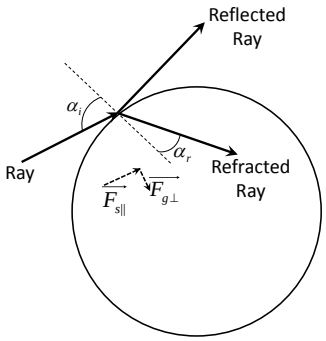

Fig. 1. Schematic of the trapping forces [11]. An incoming ray strikes a particle, applying a force that can be split into a scattering and gradient force F_s and F_g. The particle traps if it has a larger refractive index than the surrounding medium.

In an optical trap, a light beam interacts with a particle made from an optically denser material than its environment. For conditions where the particle size is comparable to or larger than the wavelength of light, a ray-optics approach is used and the beam is decomposed into a set of rays. Each ray interacts with the particle, as shown in Fig. 1; the forces due to each ray are decomposed into a scattering force F_s and a gradient force F_g. The scattering force lies parallel to the incident ray, while the gradient force is defined to be perpendicular to the incident ray.

#244048 Received 30 Jun 2015; revised 30 Aug 2015; accepted 1 Sep 2015; published 4 Sep 2015

For a single beam of small angular divergence such as that emerging from the end of an optical fiber, integration over the entire beam results in a particle that is drawn towards the axis of the beam as a result of gradient forces. For two counter-propagating beams aligned coaxially, the particle will then trap in a stable location along the beam axis due to the combination of gradient and scattering forces.

In the case where the refractive index ratio between the particle and medium is relatively large ($n_{\text{particle}}/n_{\text{medium}} > 1.01$) and the particle size satisfies the criteria for a Mie scattering treatment, $2\pi R/\lambda \gg 1$ [12], the particle will trap halfway between the two fibers in the dual beam optical trap. In this case, the scattering forces are dominant along the beam axis. The trapping location is the point where the scattering forces arising from each beam are equal in magnitude but opposite in direction, and give rise to a restoring force when the particle is displaced away from that equilibrium point along the axis. However, we have observed that this trap exhibits unusual trapping behaviors when the refractive indices between the dielectric particle and the surrounding liquid are nearly equal ($n_{\text{particle}}/n_{\text{medium}} < 1.01$). This occurs because F_s decreases more rapidly than F_g as a function of the refractive index contrast and eventually F_g becomes dominant in the axial direction as well. Our paper characterizes this behavior using samples poly(methyl methacrylate) (PMMA) beads with multiple sizes at various fiber separations. We present experimental data along with simulation results illustrating that the landscape for GUV trapping will shift between stable and unstable behavior for relevant refractive indices, fiber separations and particle sizes. By understanding trapping characteristics at low refractive index contrasts, we can increase the effectiveness of our GUV trapping apparatus and more accurately quantify the forces present within the trap.

Materials and methods

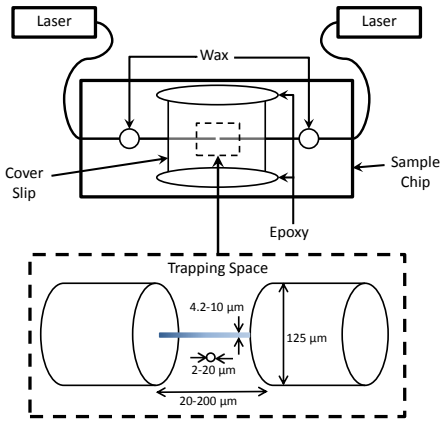

Fig. 2. Schematic of the experimental setup. The single-mode fibers are secured in place with drops of wax. A cover slip fastened with epoxy aligns the fibers in the trapping space and provides a flat field of view. The trapping space is expanded to show the relative sizes of the particles, beam and fibers. The fiber separation is fixed during chip assembly. A microscope is used to observe trapped particles and a computer controls the laser power from two separate 980 nm laser diodes.

Our dual-beam optical trap, shown in Fig. 2, utilizes two 980-nm pump lasers (Bookham LC95), which are monitored using a modular controller (Newport Model 8008) and LabVIEW software. Optical powers in the range of 50-250 mW from each fiber are typically used within

#244048 Received 30 Jun 2015; revised 30 Aug 2015; accepted 1 Sep 2015; published 4 Sep 2015

the trap. The beams are guided by single mode fibers (Fiber Instrument Sales, HI9806) to a Plexiglass sample chip (OPTIX Acrylic 1AG3622A), where the fibers are aligned along a groove. This groove is created using a 36 gauge nichrome wire (Jacobs Online NW36250) parallel to the surface and pressed down with a second Plexiglass chip, where a 0.61 A current runs through the wire for 60 s. Once the fibers are aligned to the desired separation, they are secured in the groove with household wax with a glass cover slip cut from a microscope slide to approximate dimensions of 12.5 mm $\times$ 7.0 mm and a thickness of 1.0 mm is set with five minute epoxy to ensure alignment. The microscope uses a Mitutoyo M Plan Apo 5$\times$ objective and images are recorded using a video camera attached to the eyepiece. PMMA sample droplets are placed along the glass coverslip edge, such that the sample flows through the regime due to capillary action.

Our samples consist of PMMA beads (MICROBEADS SPHEROMERS CA6, CA10, and CA15; Bangs Laboratories, Inc. Dry PMMA beads BB01N) in a refractive index liquid medium (Cargille Laboratories, Series A). The PMMA bead sizes range from 2 to 20 μm (Mie scattering according to $2\pi R/\lambda \gg 1$ applies [12]) and have a refractive index of 1.482 ± 0.002, while the medium has a refractive index of 1.4700 ± 0.0002. The sample is inserted into a 3 cc syringe and shaken well for 10 s in order to separate aggregated particles. Experiments were performed at room temperature, and we expect laser-induced heating to be minimal ($< 2^\circ$ C) [12]. Our simulations used room-temperature refractive indices and assume no thermal effects. Using the approach of Peterman *et al.*, we expect $< 2^\circ$ C of heating in the center of the trap [13].

Simulations are performed using Matlab software following the approach of Sidick *et al.* [11]. The applied force **F** on a particle by a single beam is

$$\mathbf{F} = \frac{n_{\text{medium}} P_0}{c} \mathbf{Q}, \tag{1}$$

where n_{medium} is the refractive index of the medium, P_0 is the total power transmitted by the beam, **Q** is the trapping efficiency factor of the particle, and c is the speed of light in a vacuum. For a beam centered on the particle, **Q** is reduced to a single dimension, where

$$Q_z = 2r_0^2 \int_0^{\theta_{\max}} \mathrm{d}\theta \, \sin 2\theta \, \frac{\exp(-2r^2/w^2)}{w^2} \, q_z. \tag{2}$$

Here, z indicates the axial direction, r_0 is the particle radius, θ is the angle between the normal of the surface and the beam axis, r is the distance from the surface to the beam axis, w is the beam radius, and q_z indicates the fraction of the z-component of the momentum transferred from the beam to the particle. This fraction is determined using

$$q_z = \cos(\alpha_i - \theta) + R\cos(\alpha_i + \theta) - T^2 \frac{\cos(\alpha_i + \theta - 2\alpha_r) + R\cos(\alpha_i + \theta)}{1 + R^2 + 2R\cos 2\alpha_r}, \tag{3}$$

where α_i and α_r are the angles of incidence and refraction as shown in Fig. 1, respectively, and R and T are the reflectance and transmittance at the particle surface, respectively.

For two counterpropagating beams, the force vectors from each beam are added together, such that along the beam axis, we see the net force $F_{z,\,\text{tot}}$ is

$$F_{z,\,\text{tot}} = \frac{n_1(P_1 + P_2)}{c} \left(\frac{P_1 Q_{z1}}{P_1 + P_2} - \frac{P_2 Q_{z2}}{P_1 + P_2} \right), \tag{4}$$

where subscript 1 (2) indicates a beam propagating towards the right (left). Since w is dependent on the distance from the fiber end along z, we are able to use Eq. (4) with Eqs. (2) and (3) to calculate the dependence of $Q_{z,\,\text{tot}}$ on z. By defining the fiber separation and the particle radius, we are able to see the stable and unstable trapping locations along the beam axis.

#244048 Received 30 Jun 2015; revised 30 Aug 2015; accepted 1 Sep 2015; published 4 Sep 2015

Simulation and experimental results

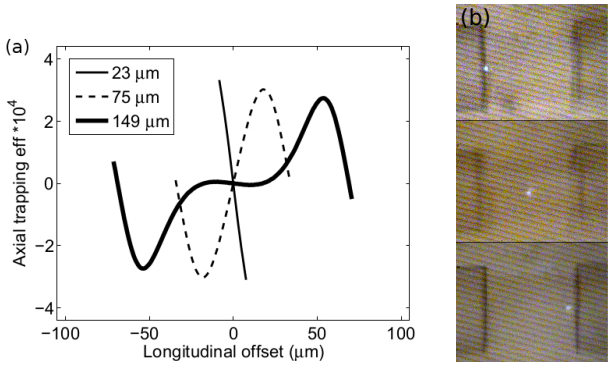

Fig. 3. (a) Simulations of the dimensionless trapping efficiency Q_z along the beam axis z when the particle radius is 3.15 μm and the fiber separation are 23 μm, 75 μm, and 149 μm. The trap center is located at $z = 0$. (b) Pictures of experimentally trapped particles at a fiber separation of 129.1 μm. The contrast and brightness were adjusted to better view the particle and fibers.

In Fig. 3(a), we present results for simulations of Q_z for particles with a 3.15-μm radius and 23-μm, 75-μm, and 149-μm fiber separations. The refractive index of the medium is 1.4700, and the refractive index of the particle is 1.482. Equilibrium locations where the net force is zero occur when $Q_z = 0$, and the stability depends on the slope of Q_z with respect to z; a stable trap will have a negative slope, while an unstable trap will have a positive slope.

The curves in Fig. 3(a) reveal three interesting phenomena for low refractive-index contrast trapping of 3.15-μm radius particles. Firstly, for small separations (23 μm) one obtains a single stable equilibrium point where the longitudinal offset is zero, which is halfway between the two fiber ends. Secondly, for intermediate separations (75 μm) one obtains an unstable equilibrium in the trap center, but two stable equilibria emerge which are located adjacent to the two optical fiber tips. Thirdly, for large separations (149 μm) one obtains three stable equilibria, one in the center and two more located adjacent to each optical fiber tip. Note that the slope of Q_z at $z = 0$ for large separations is relatively small, leading to small forces. In fact, most GUV stretching experiments are conducted for large separations ($S > 150$ μm). A key finding of our work is that it may be desirable in GUV experiments to use a configuration with smaller separations, or a single fiber because it will lead to a larger range of stretching forces. Photographs of particles for each stable trapping region are given in Fig. 3(b). The simulations for a 5-μm particle at a separation resulted in three stable equilibria, which was experimentally verified.

To further understand how a low refractive index contrast changes the behavior for a dual-beam optical trap, we compiled the Q_z simulations and created contour plots describing the trap stability at the center with varying particle sizes and fiber separation. These results are shown in Fig. 4. Here, the refractive index of the medium and particle are 1.4700 and 1.482, respectively. The contour colors depend on the slopes of Q_z for $z = 0$; a darker red indicates a larger positive slope, while a darker blue indicates a larger negative slope. The black zero line indicates the boundary between stable and unstable behavior. Our experimental observations are well-described by our model and simulations. In particular, we find that there is a wide range of particle sizes and fiber separations which lead to the possibility of both stable and unstable trapping. For example, for GUVs of 2-5 μm in radius and for fiber separations ranging from 40-250 μm one may experience small trapping forces or unstable trapping near $z = 0$, but

#244048 Received 30 Jun 2015; revised 30 Aug 2015; accepted 1 Sep 2015; published 4 Sep 2015

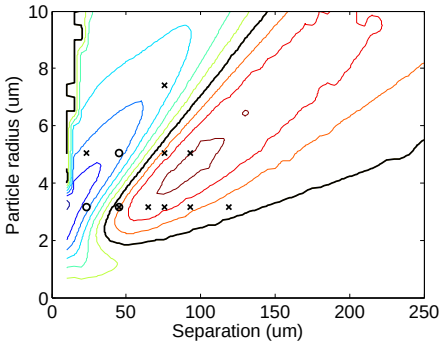

Fig. 4. Contour plot describing the expected stability at the center of the trap. The warmer colors indicate an unstable trapping regime, while the cooler colors indicate a stable trapping regime. The thick black zero line indicates location where the center is neither stable nor unstable. The contours are obtained from the simulations. Experimental data is given by markers. Open circles represent the particles observed to be trapped at $z = 0$ (indicating a stable equilibrium point at $z = 0$), while the crosses represent particles which drift away from $z = 0$ (indicating an unstable equilibrium point at $z = 0$.)

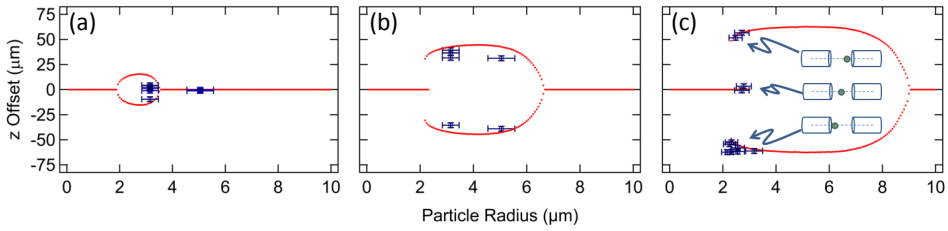

Fig. 5. Bifurcation plots showing the axial stability locations vs. particle radius for three different traps with fiber separations of (a) 45 μm, (b) 92.9 μm, and (c) 129.1 μm. The red dots represent the simulated stable trapping location, and the symbols represent experimentally observed stably trapped particles. The trap center is located at z=0. Trapping locations are shown schematically within (c). The error bars were determined empirically through measurements of the inner and outer edges of both the fiber and beads.

observe relatively large forces (about five times larger than at the center) for particles trapped adjacent to the fiber tips. In the case where the refractive index contrast between the particle and medium is large, the plot shows a larger stable trapping regime.

The Q_z simulations can also be compiled to obtain Q_z at given fiber separations for varying particle sizes and varying axial displacements of the particle, as shown in Fig. 5. The refractive index of the medium and particle are 1.4700 and 1.482, respectively for all fiber separations. We see that the bifurcation points match the zero-line position in Fig. 4. In Fig. 5(a), we see that particles with radii between 2.0 μm and 3.5 μm would not be stably trapped at the center; this applies to radii between 2.4 μm and 6.9 μm in Fig. 5(b), and between 3.0 μm and 9.0 μm in Fig. 5(c). In these "unstable ranges," the particle may be stably trapped close to the fiber ends as verified experimentally, due to F_g dominating over F_s. We also see that the unstable range increases and begins at larger particle sizes as the fiber separation increases; this can be

#244048 Received 30 Jun 2015; revised 30 Aug 2015; accepted 1 Sep 2015; published 4 Sep 2015

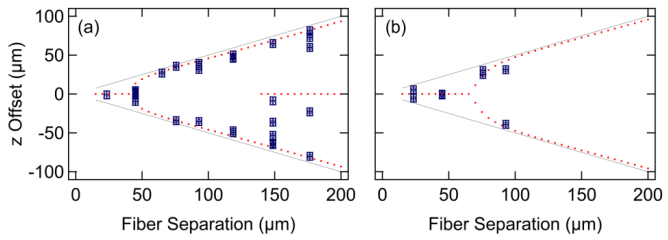

Fig. 6. Bifurcation plots of the axial stability locations as a function of fiber separation for particles of radius: (a) 3.15 μm and (b) 5.05 μm. The red dots indicate the simulated stable trapping location, the black lines show the location of the fiber ends, and the blue data points represent the observed stably trapped particles. The trap center is located at $z = 0$.

understood by considering the particle size relative to the beam diameter. When the particle radius is either much larger or smaller than the beam radius, α_i and α_r at $\theta_{\max}$ approach 0 or $\pi/2$, respectively; these result in F_s dominating over F_g. However, when the radius is within the unstable range, F_g is larger than F_s. Since the beam diameter increases as z increases and the particle interacts with both beams, at larger separations the double stable point occurs over a larger particle size range and begins at a larger size.

Interestingly, at larger separations we see sections with three stable trapping locations, as shown in Fig. 5(c) for particle radii between 2.3 μm and 3.0 μm. The three-location range is a mixture of the two scenarios; a particle entering the beam closer to the fiber ends will be pulled close to the fiber tip and trap due to the dominance of F_g in that region. On the other hand, if the particle enters the beam near the trap center, then it will trap there due to the local dominance of F_s. This is due to the z-dependence of both F_g and F_s; F_g dissipates more rapidly than F_s as a function of z, so after a certain distance the center becomes a stable point. It is important to note that the center is a weaker stable point than the ends; this is apparent in Fig. 3(a) for the 149 μm separation when comparing the stable location slopes. Therefore, the particle will more easily trap near the fiber ends, rather than the center.

Figure 5 shows data throughout the bifurcation range, but does not show data for the appearance and collapse of the bifurcation for a given fiber separation. Figure 6 on the other hand presents data for the entire range of behavior. Figure 6 maps the trap stability at a set particle size with varying fiber separations and axial displacement. Utilizing the same refractive indices, we notice the bifurcation points are located at the same position as the zero line in Fig. 4. At smaller separations, particles are stably trapped in the center due to F_s being stronger than F_g. As the separation increases, F_g begins to dominate, resulting in two stable trapping locations; this occurs at a 45 μm separation in Fig. 6(a) and a 70 μm separation in Fig. 6(b). Similar to Fig. 5, we notice the range of dual-stability locations increases, and the transition point occurs at larger separations for larger particle sizes.

In addition, analogous to Fig. 5(c), we experimentally and computationally observe a section with three stable trapping locations appearing after a 140μm-fiber separation for particles with radii of 3.15 μm, as shown in Fig. 6(a). As stated previously, this is due to the relative strengths of F_s and F_g along the z-axis; we also see the center is a weaker stable trapping location than the fiber ends, so particles will trap more easily near the fiber ends than the center.

#244048 Received 30 Jun 2015; revised 30 Aug 2015; accepted 1 Sep 2015; published 4 Sep 2015

Conclusions

We have characterized low refractive-index-contrast optical trapping in a dual-beam fiber-optical trap behavior using PMMA beads. Our simulations and experimental data show a shift between stable and unstable trapping behavior for some fiber separations and particle sizes which is due to the interplay between net gradient and net scattering forces in the axial direction. For certain fiber separations and particle sizes we find that stable trapping in the center of such a trap is not possible. When trapping near the center is possible, it is frequently accompanied by weak restoring forces in the trap. Additionally, we find that stable trapping is possible near a single fiber tip, and this single-fiber gradient force trap will exhibit a much larger restoring force (about five times larger than at the center). By understanding trapping characteristics at low refractive index contrasts, we can increase the effectiveness of our GUV trapping apparatus and more accurately quantify the forces present within the trap.

#244048 Received 30 Jun 2015; revised 30 Aug 2015; accepted 1 Sep 2015; published 4 Sep 2015